Int. J. Plasma Environ. Sci. Technol. 17 (2023) e01003 (9pp)
International Journal of Plasma Environmental Science and Technology

Regular Paper DOI: 10.34343/ijpest.2023.17.e01003

Effect of supplied gas on ROS transport through liquid targets by plasma jet irradiation

Heping Shi, Kecheng Shen, Toshiyuki Kawasaki*

Department of Electrical Engineering, Nishinippon Institute of Technology, Japan

* Corresponding author: tkawasak@nishitech.ac.jp (Toshiyuki Kawasaki)

Received: 21 November 2022
Revised: 16 February 2023
Accepted: 20 February 2023
Published online: 21 February 2023

Abstract

Recently, plasma jet technology has been developed for biomedical applications, so we must control the supply of reactive oxygen species (ROSs) by plasma to use it safely and effectively. In previous studies, several experiments were conducted using a He plasma jet. However, we have not investigated whether there is any difference when supplying different types of gas. In this study, we studied the effects of supplied gases (He and Ar) on ROS distribution in liquid and tissue models induced by plasma jet irradiation. In this experiment, we visualized the ROS distribution pattern after passing through a water layer or tissue model and obtained the relative ROS concentration profiles using absorbance measurement. The results show that the transport characteristics of ROSs produced by He or Ar plasma jets have nothing in common. We also analyzed the components of water after plasma jet irradiation.

Keywords: ROS transport, water analysis, 2-dimentsional distribution.

1. Introduction

Atmospheric pressure plasma has received extensive attention in plasma-induced reactive oxygen species (ROS) transportation, which is critical in recent plasma science and technology [1–3]. An atmospheric pressure plasma jet can be directly irradiated to target liquids, including human skin and biological tissues in atmospheric air, with no disadvantages or damages. Clarifying the interaction between plasma and liquids is important for advancing plasma science in areas where liquids are intensely involved such as plasma medicine, plasma agriculture, and water treatment. In these cases, the transportation of ROS to target cells through liquid or biomedical tissue is an important application of plasma technology. Therefore, ROS transportation through liquid targets must be investigated for the safe and effective use of this technology.

Several reports have emphasized the supply and transport of reactive species in various plasma-liquid systems [4]. In previous studies, the transport characteristics of reactive oxygen species and its penetration depth through water layers or tissue models had different effects when He gas was supplied for a cold-atmospheric plasma jet generation under different conditions [5–8]. In this experiment, we found that a two-dimensional (2D) distribution of ROS is completely different when Ar or He gas is used. We conducted different water experiments and analyzed to better understand its mechanism. Based on the water analysis difference between the Ar and He irradiated water, we discovered the reason for the different situations of ROS transportation.

2. Experimental

2.1 Plasma-jet

Fig. 1 shows schematics of the plasma generator used in this experiment. It is set up with a glass-coated rod high voltage electrode installed in the center of a glass tube with an inner diameter of 4 mm, and a ground

electrode was wrapped around the outside of the glass tube 10 mm away from the tip of the high voltage electrode. A plasma-generating gas He or Ar was supplied to the gap between the glass tube and the rod electrode at a flow rate of 3 L min^{-1} using a mass-flow controller (Kofloc 8500 MC). We used a function generator (NF WF1948) and an amplifier (Trek 10/40A) to generate high voltage. The voltages were set to 14 kV_{p-p} and 15 kV_{p-p} for He and Ar gases, respectively. The frequency was set to 10 kHz in both cases. The corresponding discharge power was approximately 3 W, as measured using an oscilloscope (Iwatsu DS-8104). The irradiation distance between the open end of the tube and the target surface was set at 10 mm.

Fig. 2 shows the typical voltage/current waveforms and discharge photographs of (a) Ar and (b) He gases.

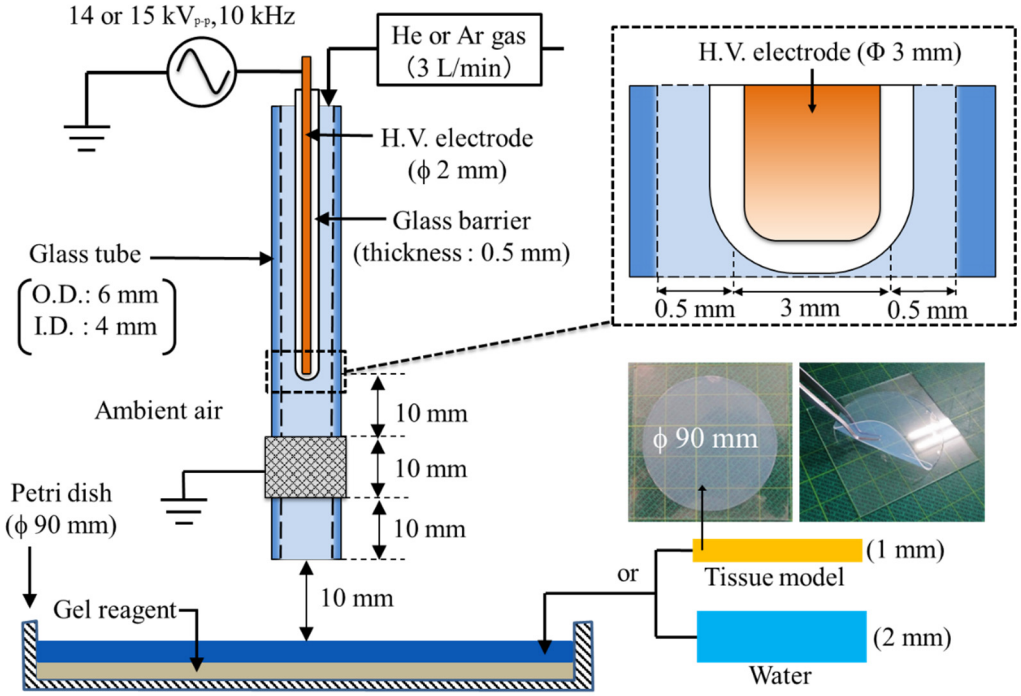

Fig. 1. Schematics of the experiment setup.

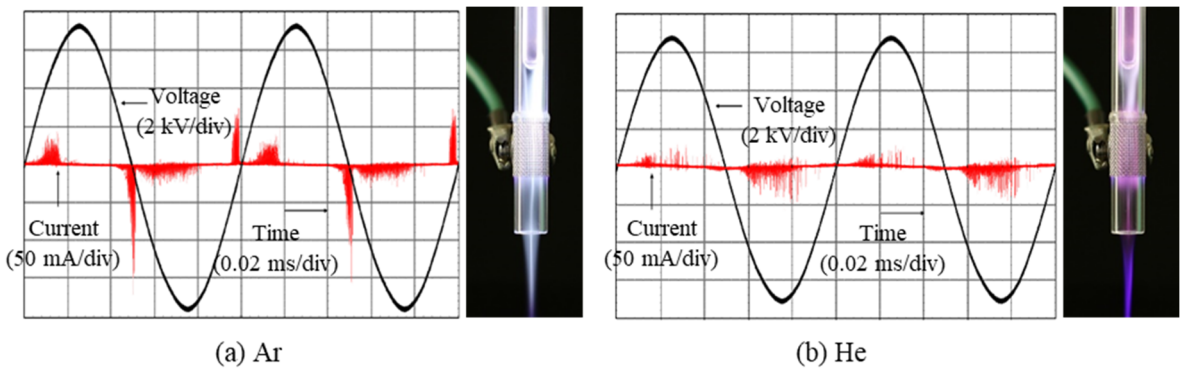

Fig. 2. Typical voltage/current waveforms and discharge photographs of (a) Ar and (b) He.

2.2 Visualization of Two-dimensional distribution

Fig. 3 (a) shows the KI-starch gel ROS detection reagent for determining the 2D distribution of ROS. This reagent was divided into 20-g portions in Petri dishes with a diameter of 90 mm. The KI-starch gel ROS detection reagent undergoes an oxidation reaction with the active species generated by plasma irradiation, resulting in a purple color change. An example of the color reaction is shown in Fig. 3 (b).

To obtain the ROS distribution through several layers, we first irradiated the KI-starch gel reagent for 5 s directly, then measured the reagent absorbance [9-12]. We also prepared distilled water at a thickness of 2 mm using the KI-starch gel reagent [13]. The surfaces of the water layer are irradiated with a plasma jet under open-air conditions. The ROS are transported through the water layer to the KI-starch gel reagent in a 15-min

plasma irradiation. Then, the water was removed from the KI-starch gel reagent after irradiation, and we visualize the ROS distribution patterns after plasma irradiation. In addition, we used agarose (0.4%) as the tissue model (thickness: 1 mm) irradiated by plasma jet for five min and stand by plasma-off for five min, then removed the tissue model, and finally, the color reaction of the KI-starch reagent was observed.

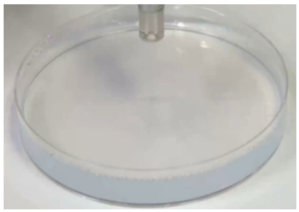

(a) Before irradiation

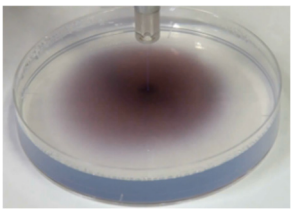

(b) After irradiation

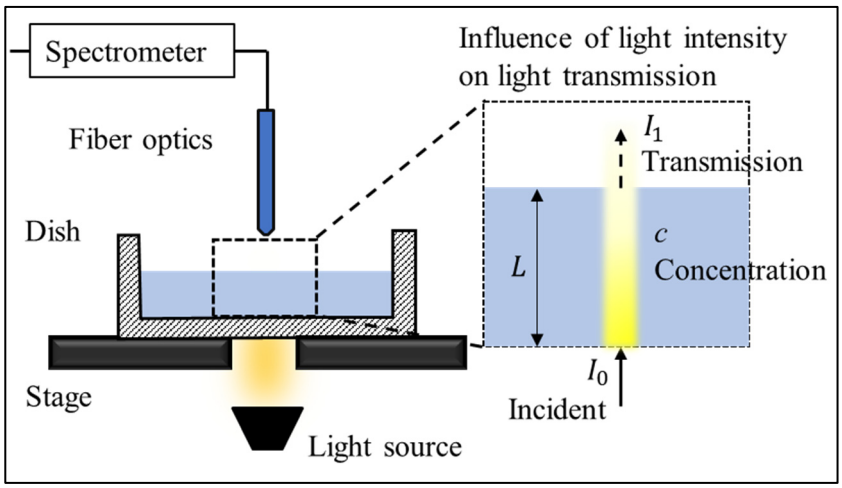

(c) Absorbance measurement to obtain relative ROS concentration

Fig. 3. Two-dimensional measurement system for gel reagent (a) before and (b) after plasma irradiation, (c) absorbance measurement to obtain relative ROS concentration.

Fig. 3 (c) shows the 2D measurement system used in our laboratory to measure the absorbance of the color reaction. After plasma irradiation, the gel-like ROS detection reagent is irradiated by a light source simulating sunlight underneath, and the relative ROS concentration was measured using the Beer-Lambert law from the transmitted light and the light intensity of the light source. A common and practical expression of the Beer-Lambert law relates the optical attenuation of a physical material containing a single attenuating species of uniform concentration to the optical path length through the sample and absorptivity of the species. This expression is as follows:

$$\boldsymbol{A(Absorbance)} = -\log_{10}\left(\frac{I_1}{I_0}\right) = \varepsilon Lc \qquad (1)$$

where A is the absorbance, ε is the molar attenuation coefficient or absorptivity of the attenuating species, L is the optical path length in cm, c is the concentration of the attenuating species, I_1 is the radiant flux transmitted by the material sample, I_0 is the radiant flux received by the material sample.

In this experiment, ε and L are constant values, so the relative ROS concentration can be obtained from the absorbance.

2.3 Water analysis

In this experiment, we prepared 40 ml of distilled water in the same Petri dishes. Then, we irradiated the surface of the liquid. The irradiation time was varied from 5 to 30 min to determine what happened in the liquid after plasma irradiation. We used densitometers (Kyoritsu chemical-check lab) and absorption photometry with a chromogenic reagent to measure the concentration of hydrogen peroxide (densitometers: DPM2-H_2O_2, reagent: WAK-H_2O_2) and nitrous acid (densitometers: DPM2-NO_2, reagent: WAK-NO_2). We also measured the pH and liquid conductivity of the water after plasma irradiation.

3. Results and discussion

In this study, some ROS generated by plasma irradiation can reach the target through the liquid. Therefore, focused on the distribution of transported ROS through liquids by plasma irradiation.

Fig. 4 shows the result of a 2D distribution experiment in air without any water or water layers. A visualization of the oxidation reaction on the target surface in the air is shown in Figs. 4 (a) and 4 (b). The color reaction of the KI-starch reagent using an Ar plasma jet is shown in Fig. 4 (a), and the color reaction by the He plasma jet is shown in Fig. 4 (b). The color reaction of the Ar plasma generator is different from that of the He plasma generator. Fig. 4 (a) shows a small color reaction at the center of the KI-starch reagent, and two bigger circular color reactions around the center. While Fig. 4 (b) shows only a small circle at the center of the KI-starch reagent. Based on the color reaction results, we obtained the relative ROS concentration distributions by measuring the absorbance along lines A to B (Figs. 4 (a) and 4 (b)). The relative ROS concentrations when the surface of the KI-starch reagent is irradiated with an Ar or He plasma generator under open-air conditions are shown in Fig. 4 (c).

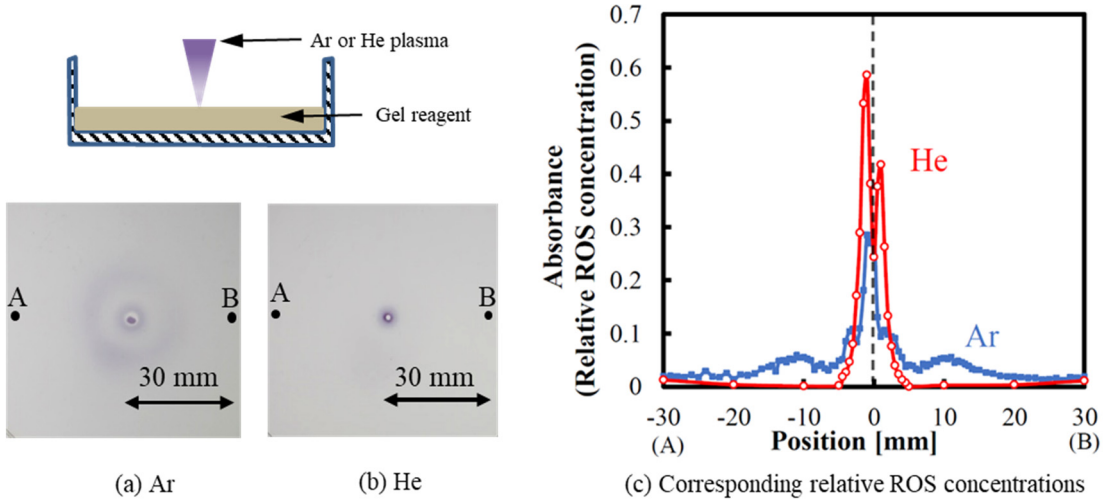

Fig. 4. Results of two-dimensional distribution experiment without a water layer or tissue model for (a) Ar gas, (b) He gas, and (c) corresponding relative ROS concentration obtained by absorbance measurement along the AB lines.

Fig. 5 shows the result of a 2D distribution experiment through the water. The visualization of the oxidation reaction on the target surface through water is shown in Figs. 5 (a) and 5 (b). The color reaction of the KI-starch reagent using an Ar plasma jet is shown in Fig. 5 (a), while the color reaction by the He plasma jet is shown in Fig. 5 (b). The color reaction takes the shape of donuts when using the Ar plasma generator (Figs. 5(a) and 5 (b)). However, the color reaction cannot be observed when using the He plasma generator in this experiment.

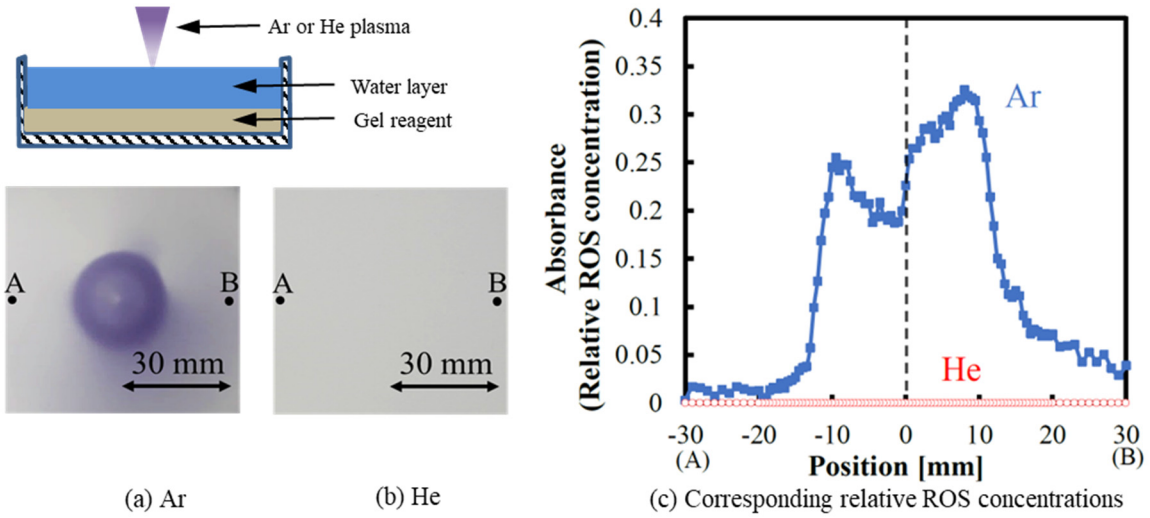

Fig. 5. Results of two-dimensional distribution experiment through the water layer for (a) Ar gas, (b) He gas and (c) corresponding relative ROS concentrations obtained by absorbance measurement along the AB lines.

Based on the color reaction results, we obtained the relative ROS concentration distributions by measuring the absorbance along lines A to B (Figs. 5 (a) and 5 (b)). The relative ROS concentration transported through the water layer to reach the KI-starch gel reagent beneath when the surface of the water layer is irradiated with an Ar or He plasma generator under open-air conditions is shown in Fig. 5 (c).

Fig. 6 shows the result of the 2D distribution experiment through a tissue model. A visualization of the oxidation reaction on the target surface is shown in Figs. 6 (a) and 6 (b). The color reaction of the KI-starch reagent using an Ar plasma jet is shown in Fig. 6 (a), while the color reaction by the He plasma jet is shown in Fig. 6 (b). The color reaction by the Ar plasma generator is different from that by the He plasma generator. A dark and circular color reaction could be observed at the center of the KI-starch reagent (Fig. 6 (a)), whereas only a thick and circular color reaction could be observed at the center of the KI-starch reagent (Fig. 6 (b)). Based on the color reaction results, we obtained the relative ROS concentration distributions by measuring the absorbance along lines A to B (Figs. 6 (a) and 6 (b)). The relative ROS concentrations when the surface of the tissue model is irradiated with a plasma generator under open-air conditions are shown in Fig. 6 (c).

Comparing the 2D distribution results of Ar plasma irradiation with the results of He plasma irradiation, we found some differences between Ar and He plasma. For the color reaction results of water layers shown in Fig. 5, it has been reported that this donut-shaped distribution is related to the plasma-induced flow [13, 14]. The transport of ROS through water layer is affected by the plasma-induced flows. And in this experiment, the plasma-induced flows may cause the diffusion of ROS in water easily because of the low viscosity of water. However, for the color reaction results of tissue models shown in Fig. 6, the transport of ROS through tissue model in this experiment is hard to spread because of the high viscosity of tissue model. Based on the results of two-dimensional distribution, we focused on plasma differences through the water layer. We investigated the ROS supplied or produced by Ar plasma irradiation transport to the bottom of the liquid (Fig. 5 (a)). However, we cannot observe anything on the surface of the KI-starch reagent (Fig. 5 (b)). To explain these phenomena, we analyzed the liquid component after Ar or He plasma jet irradiation.

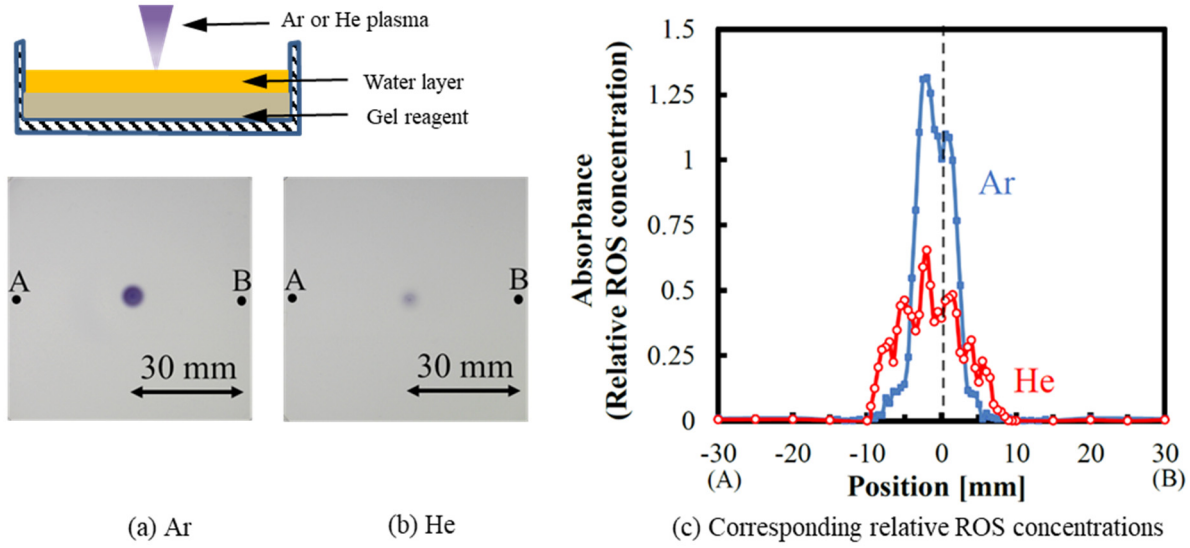

Fig. 6. Results of two-dimensional distribution experiment through the tissue model for (a) Ar gas, (b) He gas and (c) corresponding relative ROS concentrations obtained by absorbance measurement along the AB lines.

In previous studies, Ar and He plasma, upon contact with water, initiate the chemical reaction that generates ROS such as OH radical to produce hydrogen peroxide. It also generates RNS variations due to the interaction with the surrounding atmosphere to produce NO_2^- and NO_3^-. The collision of the electrons can produce the following reactions [15]:

$$Ar + e \rightarrow Ar^* + e \quad (2) \quad [16]$$

$$He + e \rightarrow He^* + e \quad (3) \quad [17]$$

$$O_2 + e \rightarrow 2O + e \quad (4) \quad [18]$$

$$N_2 + e \rightarrow 2N + e \quad (5) \quad [19]$$

$$H_2O + e \rightarrow H^{\cdot} + HO^{\bullet} + e \quad (6) \quad [20]$$

Aqueous and gaseous hydrogen peroxide can result from the recombination of two hydroxyl radicals in a liquid.

$$Ar^* + H_2O \rightarrow Ar + H^{\cdot} + HO^{\cdot} \quad (7) \quad [16]$$

$$He^* + H_2O \rightarrow He + H^{\cdot} + HO^{\cdot} \quad (8) \quad [21]$$

$$2N + 2H_2O \rightarrow N_2 + 2H^{\cdot} + 2HO^{\cdot} \quad (9) \quad [22]$$

$$O + H_2O \rightarrow 2HO^{\cdot} \quad (10) \quad [23]$$

$$HO^{\cdot} + HO^{\cdot} \rightarrow H_2O_2 \quad (11) \quad [24]$$

The untypical trend of nitrite concentration in water during plasma activation is the result of a competition between nitrites and nitrates produced in a hermetic enclosure [23]. The formation of nitrogen oxide in the gas phase is described by the Zeldovich reactions. In the atmospheric plasma, NO is rapidly turned into nitrogen dioxide by three reactions with oxygen. In the second phase, nitrogen dioxide is dissolved in water, resulting in the formation of nitrites, nitrates, and hydronium ions [25].

$$N + O \rightarrow NO + N \quad (12) \quad [26]$$

$$N + O \rightarrow NO + O \quad (13) \quad [26]$$

$$NO + O^{\cdot} + M \rightarrow NO_2 + M \quad (14) \quad [26]$$

$$2NO_2 + H_2O \rightarrow NO_2^- + NO_3 + 2H^+ \quad (15) \quad [27]$$

$$NO + NO_2 + H_2O \rightarrow 2NO_2^- + 2H^+ \quad (16) \quad [28]$$

Consequently, the rate of nitrite production decreases with activation time while two reactions transform nitrites into nitrates using O_3, as follows:

$$NO_2^- + O_3 \rightarrow NO_3^- + O_2 \quad (17) \quad [27,29]$$

The chemical reactions mentioned here are well known as representative chemical reactions in the interaction between the plasma irradiation and the liquid phase, as in this experiment. Therefore, we focused on the concentration of hydrogen peroxide and nitrous acid in water after plasma irradiation in this experiment.

Figs. 7 (a) and 7 (b) show the concentration of nitrous acid and hydrogen peroxide after plasma irradiation for 5 to 30 min, respectively. The results of the color reaction of the chromogenic reagent are shown in Figs. 7(a) and 7 (b). The concentration of nitrous acid and hydrogen peroxide after Ar plasma irradiation is higher than the results after He plasma irradiation (Figs. 7 (a) and 7 (b)). In addition, the liquid conductivity and pH of the liquid after plasma irradiation are shown in Figs. 7 (c) and 7 (d), respectively. The liquid conductivity after Ar plasma irradiation is higher than the results after He plasma irradiation, while the pH after Ar plasma irradiation is lower than the results after He plasma irradiation.

Several reports have shown that the number of OH radicals generated using Ar plasma is greater than the results generated using He plasma [1]. Ar plasma jet provides higher efficiency in generating hydrogen peroxide [30], as well as more ozone and nitrogen oxides than He plasma jets [31]. Therefore, the results of the water analysis in this experiment can be confirmed using these reports.

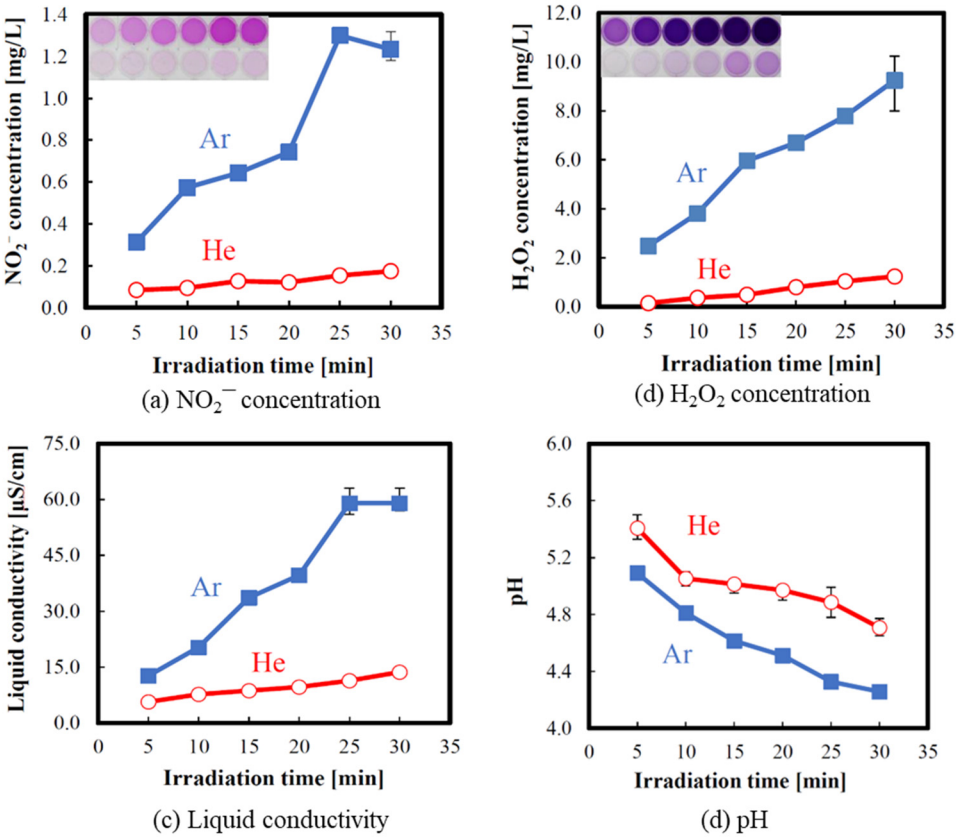

Fig. 7. Results of water analysis for (a) NO_2^- concentration, (b) H_2O_2 concentration, (c) liquid conductivity and (d) pH of water by plasma irradiation from 5 to 30 mins.

Based on the results of the water analysis, there was a correlation between ROS transport and the results of the water analysis. We can understand that there are more ROS transported to the bottom through water layer or tissue model when supply Ar gas. Therefore, the ROS does not have enough power to be transported deeply when using a He plasma jet.

However, the results of irradiation in air without a water layer or tissue model as shown in Fig. 4, it does not mean the He plasma jet provides less concentration of ROS than the plasma generated by Ar gas. Since these relationships cannot be explained at present, this will be a subject for our future work.

4. Conclusion

In this study, we investigated the effect of the supplied gas on ROS transport in the liquid after plasma jet irradiation. Under the present experimental conditions, the amount of ROS that reached the bottom of the water layer or tissue model transported by Ar plasma jet is larger than the results by He plasma jet. In addition, water analysis experiments were performed, and there was a correlation between the ROS transport and the amount of hydrogen peroxide or nitrous acid in the liquid produced by plasma irradiation. In conclusion of the comparison, hydrogen peroxide and nitrous acid generated or supplied by plasma irradiation promote ROS transport toward the depth direction in liquids.

References

[1] Xu D., Liu D., Wang B., Chen C., Chen Z., Li D., Yang Y., Chen H., and Kong M. G., In Situ OH generation from O_2^- and H_2O_2 plays a critical role in plasma-induced cell death, *PLoS ONE*, Vol. 10 (6), e0128205, 2015.

[2] Norberg S. A., Tian W., Johnsen E., and Kushner M. J., Atmospheric pressure plasma jets interacting with liquid covered tissue: touching and not-touching the liquid, *J. Phys. D: Appl. Phys*. Vol. 47 (47), 475203, 2014.

[3] Gils C. A. J. van, Hofmann S., Boekema B. K. H. L., Brandenburg R., and Bruggeman P. J., Mechanisms of bacterial inactivation in the liquid phase induced by a remote RF cold atmospheric pressure plasma jet, *J. Phys. D: Appl. Phys*., Vol. 46 (17), 175203, 2013.
[4] P. J. Bruggeman, M. J. Kushner, B. R. Locke, J. G. E. Gardeniers, W. G. Graham, D. B. Graves, R. C. H. M. Hofman-Caris, D. Maric, J. P. Reid, and E. Ceriani, Plasma–liquid interactions: a review and roadmap, *Plasma Sources Sci. Technol*., Vol. 25 (5), 053002, 2016.
[5] Thulliez M., Bastin O., Nonclercq A., Delchambre A., and Reniers F., Gel models to assess distribution and diffusion of reactive species from cold atmospheric plasma: an overview for plasma medicine applications, *J. Phys. D: Appl. Phys*., Vol. 54 (46), 463001, 2021.
[6] Kawasaki T., Fumiaki M., Koga K., and Shiratani M., Local supply of reactive oxygen species into a tissue model by atmospheric-pressure plasma-jet exposure, *J. Appl. Phys*., Vol. 125, 213303, 2019.
[7] Kawasaki T., Kuroeda G., Sei R., Yamaguchi M., Yoshinaga R., Yamashita R., Tasaki H., Koga K., and Shiratani M., Transportation of reactive oxygen species in a tissue phantom after plasma irradiation, *Jpn. J. Appl. Phys*., Vol. 57, 01AG01, 2018.
[8] Kawasaki T., Sato A., Kusumegi S., Kudo A., Sakanoshita T., Tsurumaru T., Uchida G., Koga K., and Shiratani M., Two-dimensional concentration distribution of reactive oxygen species transported through a tissue phantom by atmospheric-pressure plasma-jet irradiation, *Appl. Phys Express*., Vol. 9, 076202, 2016.
[9] Kawasaki T., Kawano K., Mizoguchi H., Yano Y., Yamashita K., Sakai M., Uchida G., Koga K., and Shiratani M., Control of the area irradiated by the sheet-type plasma jet in atmospheric pressure, *J. Phys.: Conf. Ser.*, Vol. 518, 012016, 2014.
[10] Kawasaki T., Kawano K., Mizoguchi H., Yano Y., Yamashita K., Sakai M., Shimizu T., Uchida G., Koga K., and Shiratani M., Visualization of the distribution of oxidizing substances in an atmospheric pressure plasma jet, *IEEE Trans. Plasma Sci.*, Vol. 42 (10), pp. 2482−2483, 2014.
[11] Nakajima A., Uchida G., Kawasaki T., Koga K., Sarinont T., Amano T., Takenaka K., Shiratani M., and Setsuhara Y., Effects of gas flow on oxidation reaction in liquid induced by He/O_2 plasma-jet irradiation, *J. Appl. Phys.*, Vol. 118, 043301, 2015.
[12] Kawasaki T., Kawano K., Mizoguchi H., Yano Y., Yamashita K., and Sakai M., Visualization of the two-dimensional distribution of ROS supplied to a water-containing target by a non-thermal plasma jet, *Int. J. Plasma Environ. Sci. Technol.*, Vol. 10 (1), pp. 41−46, 2016.
[13] Kawasaki T., Eto W., Hamada M., Wakabayashi Y., Abe Y., and Kihara K., Detection of reactive oxygen species supplied into the water bottom by atmospheric non-thermal plasma jet using iodine-starch reaction, *Jpn. J. Appl. Phys*., Vol. 54 (1), 086201, 2015.
[14] Kawasaki T., Kusumegi S., Kudo A., Sakanoshita T., Tsurumaru T., and Sato A., Effects of gas flow rate on supply of reactive oxygen species into a target through liquid layer in cold plasma jet, *IEEE Trans. Plasma Sci.*, Vol. 44 (12), pp. 3223−3229, 2016.
[15] Takamatsu T., Uehara K., Sasaki Y., Miyahara H., Matsumura Y., Iwasawa A., Ito N., Azuma T., Kohno M., and Okino A., Investigation of reactive species using various gas plasmas, *RSC Adv*., Vol. 4, pp. 39901−39905, 2014.
[16] Mason R. S., Miller P. D., and Mortimer I. P., Anomalous loss of ionization in argon-hydrogen plasma studied by fast flow glow discharge mass spectrometry, *Phys. Rev. E*, Vol. 55 (6), pp. 7462−7472, 1997.
[17] Karakas E., Koklu M., and Laroussi M., Correlation between helium mole fraction and plasma bullet propagation in low temperature plasma jets, *J. Phys. D: Appl. Phys.*, Vol. 43 (15), 155202, 2010.
[18] Bian W., Song X., Liu D., Zhang J., and Chen X., Actions of nitrogen plasma in the 4-chrolophenol degradation by pulsed high-voltage discharge with bubbling gas, *Chem. Eng. J*., Vol. 219, pp. 385−394, 2013.
[19] Sharma V., Hosoi K., Mori T., and Kuroda S., Effects of Cold Atmospheric Pressure Plasma Jeton the Viability of Bacillus subtilis Endospores, *Advanced Materials Research*, Vol. 647, pp. 524−531, 2013.
[20] Liu D. X., Bruggeman P., Iza F., Rong M. Z., and Kong M. G., Global model of low-temperature atmospheric-pressure He + H_2O plasmas, *Plasma Sources Sci. Technol*., Vol. 19 (2), 025018, 2010.
[21] Li M., Xu G. H., Tian Y. L., Chen L. and Fu H. F., Carbon dioxide reforming of methane using DC corona discharge plasma reaction, *J. Phys. Chem. A*., Vol. 108 (10), pp. 1687−1693, 2004.
[22] Moravej M., Yang X., Barankin M., Penelon J., Babayan S. E., and Hicks R. F., Properties of an atmospheric pressure radio-frequency argon and nitrogen plasma, *Plasma Sources Sci. Technol*., Vol. 15 (2), pp. 204−210, 2006.
[23] Kongmany S., Matsuura H., Furuta M., Okuda S., Imamura K., and Maeda Y., Plasma application for detoxification of Jatropha phorbol esters, *J. Phys*.: *Conf. Series*, Vol. 441, 012006, 2013.
[24] Judée F., Simon S., Bailly C., and Dufour T., Plasma-activation of tap water using DBD for agronomy applications: Identification and quantification of long lifetime chemical species and production/consumption mechanisms, *Water Res.*, Vol. 133, pp. 47−59, 2018.
[25] Maheux S., Duday D., Belmonte T., Penny C., Cauchie H.M., Clément F., and Choquet P., Formation of ammonium in saline solution treated by nanosecond pulsed cold atmospheric microplasma: a route to fast inactivation of E. coli bacteria, *RSC. Adv.*, Vol. 5, 42135, 2015.

[26] Fridman A., Plasma chemistry, Cambridge University Press. New York, pp. 415, 2008.
[27] Liu D. X., Liu Z.C., Chen C., Yang A.J., Li D., Rong M.Z., Chen H.L., and Kong M.G., Aqueous reactive species induced by a surface air discharge: Heterogeneous mass transfer and liquid chemistry pathways. *Sci. Rep.,* Vol. 6, 23737, 2016.
[28] Vanraes P., Ghodbane H., Davister D., Wardenier N., Nikiforov A., Verheust Y.P., Van Hulle S.W.H., Hamdaoui O., Vandamme J., Van Durme J., Surmont P., Lynen F., and Leys C., Removal of several pesticides in a falling water film DBD reactor with activated carbon textile: Energy efficiency. *Water Res.*, Vol. 116, pp. 1−12, 2017.
[29] Van Gaens W. and Bogaerts A., Kinetic modelling for an atmospheric pressure argon plasma jet in humid air. *J. Phys. D: Appl. Phys.*, Vol. 46 (27), 275301, 2013.
[30] Ogawa K., Oh J., Gaur N., Hong S., Kunta H., Akira M., Hatta A., Robert D. Short, Ito M., and Endre J. Szili, Modulating the concentrations of reactive oxygen and nitrogen species and oxygen in water with helium and argon gas and plasma jets, *Jpn. J. Appl. Phys.*, Vol. 58, SAAB01, 2019.
[31] Nastuta A.V. and Gerling T., Cold atmospheric pressure plasma jet operated in Ar and He: From basic plasma properties to vacuum ultraviolet, electric field and safety thresholds measurements in plasma medicine, *Appl. Sci.*, Vol. 12 (2), 644, 2022.